ELSEVIER

Journal of African Earth Sciences 37 (2003) 313–330

Journal of African Earth Sciences

www.elsevier.com/locate/jafrearsci

An example of post-collisional mafic magmatism: the gabbro–anorthosite layered complex from the Tin Zebane area (western Hoggar, Algeria)

Saïda Aït-Djafer [a], Khadidja Ouzegane [a], Jean Paul-Liégeois [b,*], Jean Robert Kienast [c]

[a] *Laboratoire de Géodynamique, Géologie de l'Ingénieur et de Planétologie, U.S.T.H.B, B.P. 32 El Alia Algiers, Algeria*
[b] *Isotope Geology, Africa Museum, B-3080 Tervuren, Belgium*
[c] *Laboratoire de Pétrologie, CNRS UMR 7097 IPGP, Université de Paris 7, Tour 26-O, 4 place Jussieu, 75252 Paris, France*

Received 20 October 2002; accepted 16 June 2003

Abstract

The Tin Zebane gabbro–anorthosite layered mafic intrusion represented by plagioclase-rich cumulates forms a set of small lenticular to round-shaped mainly undeformed bodies intruding the Pan-African high-pressure metamorphic rocks from western Hoggar (Tuareg shield, southwest Algeria). The coarse-grained anorthosites are mainly made of slightly zoned bytownite ($An_{86–74}$) with the higher anorthite content at the cores. Anorthosites are interlayered with leucogabbros and gabbros that show preserved magmatic structures and with olivine gabbros characterised by coronitic textures. The primary assemblage in gabbros includes plagioclase ($An_{93–70}$), olivine ($Fo_{77–70}$), zoned clinopyroxene ($En_{43–48}Fs_{05–13}Wo_{41–49}$ with Al_2O_3 up to 4.3 wt.%) and rare orthopyroxene ($En_{73–78}$). Pyroxenes and olivine are commonly surrounded by Ca-amphibole. The olivine–plagioclase contact is usually marked by a fine orthopyroxene–Cr-spinel–amphibole symplectite. A magnesian pigeonite ($En_{70–75}Fs_{19–20}Wo_{6–10}$) is also involved in corona. The coronitic minerals have equilibrated with the primary mineral rims at P–T–a_{H2O} conditions of 797 ± 42 °C for $a_{H2O} = 0.5$ and 808 ± 44 °C for $a_{H2O} = 0.6$ at 6.2 ± 1.4 kbar. The Tin Zebane gabbroic rocks are depleted in REE with a positive Eu anomaly, high Sr (>10 * chondrite) and Al_2O_3 concentrations (17–33%) that support plagioclase accumulation with the extreme case represented by the anorthosites. The REE patterns can be modelised using plagioclase, clinopyroxene and orthopyroxene REE signature, without any role played by accessory minerals. High MgO content points to olivine as a major cumulate phase. Anorthositic gabbros Sr and Nd isotopic initial ratios are typical of a depleted mantle source ($Sr_i = 0.70257–0.70278$; $\varepsilon_{Nd} = +5.9$ to $+7.8$). This isotopic signature is identical to that of the 10-km wide 592 Ma old dyke complex composed of alkaline to peralkaline granites and tholeiitic gabbros and one single bimodal complex can be inferred. The source of the Tin Zebane basic rocks corresponds to the prevalent mantle (PREMA). The Tin Zebane complex was emplaced along the mega-shear zone bounding to the west the Archaean In Ouzzal metacraton. The model proposed suggests a linear lithospheric delamination along this rigid and cold terrane due to post-collisional transtensional movements. This allowed the asthenosphere to rise rapidly and to melt by adiabatic pressure release. Transtension along a rigid body allowed these mantle melts to reach the surface rapidly without any crustal contamination.

Keywords: Anorthosite; Gabbro; Layered mafic intrusion; Pan-African orogeny; Hoggar

1. Introduction

The Tuareg shield comprises the Hoggar, the Adrar des Iforas and the Aïr regions (Fig. 1) and constitutes the northern part of the Trans-Saharan Pan-African belt of West Africa. The Tuareg shield is formed by 23 displaced terranes. The identified terranes were juxtaposed by north–south oriented strike-slip mega-shear zones of hundreds kilometres long during the Pan-African orogeny (750–550 Ma, Black et al., 1994; Fig. 1). Terranes boundaries are either marked by ophiolitic assemblages and molassic deposits (Black et al., 1994) or by alkaline–peralkaline granitoids (Liégeois et al., 1998; Hadj-Kaddour et al., 1998) locally associated with mafic–ultramafic bodies (Black et al., 1994). The Tuareg shield amalgamation during the Neoproterozoic comprises different island arc accretions, including thrusting

* Corresponding author. Tel./fax: +32-2-650-2252.
E-mail addresses: carmanache@hotmail.com (S. Aït-Djafer), jean.paul.liegeois@africamuseum.be (J. Paul-Liégeois), jrk@ccr.jussieu.fr (J.R. Kienast).

0899-5362/$ - see front matter © 2003 Elsevier Ltd. All rights reserved.
doi:10.1016/j.jafrearsci.2003.06.001

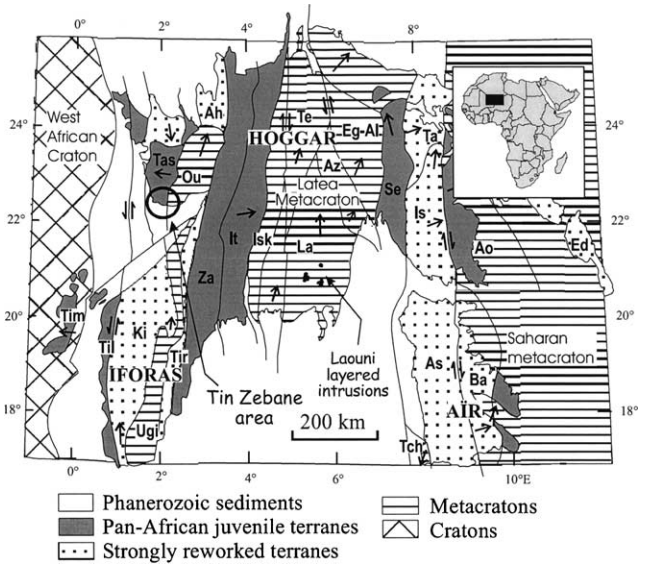

Fig. 1. Tuareg shield terrane map (from Black et al., 1994; West Africa) with location of Tin Zebane area. Solid arrow = movement direction. From east to west, the 23 terranes are Djanet (Dj), Edembo (Ed), Aouzegueur (Ao), Barghot (Ba), Assodé-Issalane (As-Is), Tchilit (Tch), Tazat (Ta), Serouenout (Se), Egéré-Aleksod (Eg-Al), Azrou-n-Fad (Az), Tefedest (Te), Laouni (La), Iskel (Isk), In Teidini (It), Tin Zaouatene (Za), Tirek (Tir), Ahnet (Ah), In Ouzzal (Ou), Iforas granulitic unit (Ugi), Tassendjanet (Tas), Kidal (Ki), Tilemsi (Til), Timétrine (Tim).

of high-pressure eclogitic rocks in some cases, at ca. 850 Ma, 720 Ma, 685 Ma, 630 Ma (Liégeois et al., 2003, and references therein). The main closure event, which finally led to the end of the orogeny, corresponds to the oblique collision with the West African Craton (Black et al., 1979). This major event induced a general northward migration of the Tuareg terranes along N–S mega-shear zones and along mega-thrusts, which was accompanied by abundant post-collisional high-K calc-alkaline post-collisional intrusions and high temperature regional metamorphism (mainly 620–580 Ma; Liégeois et al., 1994, 1998, 2003).

The end of the post-collision period is marked by the emplacement of alkaline–peralkaline dyke swarms, plateau lavas and ring complexes to the west of the shield (Liégeois et al., 1987; Hadj-Kaddour et al., 1998) and of alkali-calcic high-level plutons in the centre of the shield (''Taourirt'' province; Boissonnas, 1974; Azzouni-Sekkal et al., 2003). This diachronic event corresponds to the waning stages of shearing along mega-shear zones (Liégeois et al., 1987, 1994, 1998) during a stress-field inversion (Boullier et al., 1986), passing from transpression to transtension.

Previous study of post-collisional magmatism in the Tuareg shield have been mostly focused on granites (Liégeois et al., 1998 and references therein), while tholeiitic mafic and ultramafic layered intrusions have received only minor attention. Among the latter, the mafic intrusions from the south of the Tuareg shield have been interpreted as a post-collisional magmatism (Laouni mafic–ultramafic layered intrusions, Cottin et al., 1998; Fig. 1). Tholeiitic gabbros within the Tin Zebane dyke swarm, in the west of the Tuareg shield, have been genetically related to alkaline–peralkaline granitic rocks (Dostal et al., 1979; Hadj-Kaddour et al., 1998; Fig. 2).

This paper presents a description of the newly discovered gabbro–anorthosite complex at the northern part of the Tin Zebane area (Fig. 2), just to the north of the major dyke swarm described by Hadj-Kaddour et al. (1998). This layered gabbro–anorthosite complex intruded after the collision-related high-pressure Pan-African metamorphism in the Western Hoggar (Fig. 2). The study focuses on the textural reaction interpretation, on the mineral chemistry with determination of *P–T* conditions from minerals in equilibrium, and on the origin of corona. These basic cumulate rocks can be linked to the granitoids on the basis of whole-rock geochemical and Sr–Nd isotopic ratios analyses. This allows to constrain the implication of anorthosites formation for alkaline–peralkaline magma differentiation.

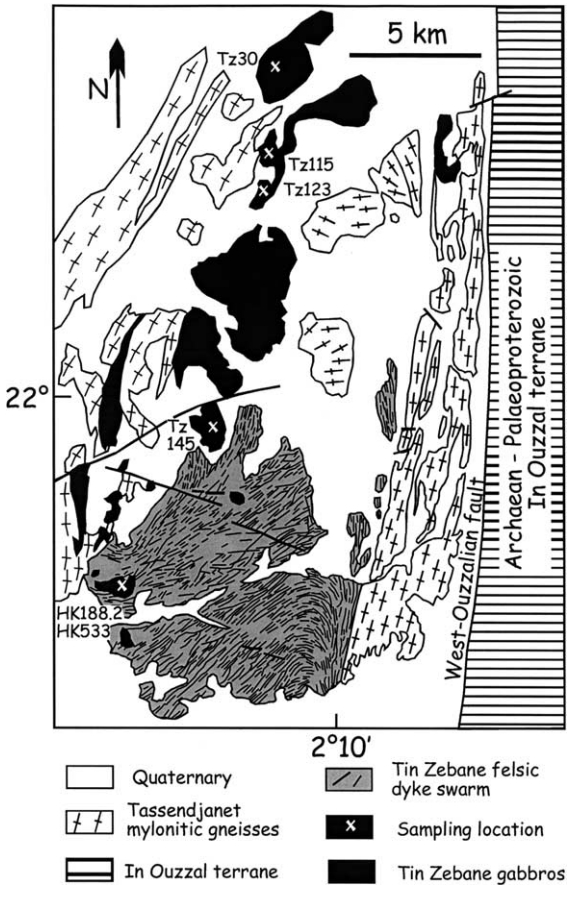

Fig. 2. Schematic geological map of Tin Zebane after Dostal et al. (1979) and Hadj-Kaddour et al. (1998) with location of the studied samples.

In addition, the new data address the potential link between layered mafic rocks and granitoids from the Tuareg shield (Laouni complexes, Cottin et al., 1998 and "Taourirt" granitoids, Azzouni-Sekkal et al., 2003) and constrain the end of the Pan-African orogeny in the Tuareg shield.

2. Geological setting and lithology

A sketch geological map of the Tin Zebane area is shown in Fig. 2. This area belongs to the Tassendjanet terrane situated in the western part of the Hoggar shield. The Tassendjanet terrane is composed of an Eburnian gneissic basement covered by orthoquartzites and alkaline metarhyolites dated at 1750 Ma (Caby and Andreopoulos-Renaud, 1983; Caby and Monié, 2003) and by an early Neoproterozoic platform stromatolites series (<1000 Ma) intruded by a gabbroic and ultramafic intrusion at about 790 Ma (Dostal et al., 1996). The latter were reworked into a thick unit composed of volcanic greywackes and plutonic-pebble conglomerates with intercalation of volcanic rocks; these series called the "Green Series" are dated at 690–630 Ma and are considered to have been generated during a subduction period (Caby et al., 1989). The Tassendjanet terrane is moreover characterised by major thrusts and high-pressure (eclogites) metamorphism which resulted from the oblique collision between the Tuareg shield and the West African craton (Caby, 1970; Caby and Monié, 2003). This high pressure metamorphism is not dated but the eclogites in the Gourma area (SW of Adrar des Iforas) linked to the same collisional event have been dated at ca. 623 Ma (Ar–Ar on phengite, confirmed by Sm–Nd isochron on minerals; Jahn et al., 2001).

The In Ouzzal terrane is located just east of the Tassendjanet terrane, the two terranes being separated by the West-Ouzzalian mega-shear zone (Figs. 1 and 2). This terrane is composed of Archaean to Palaeoproterozoic rocks affected by a high temperature granulitic metamorphism (Kienast and Ouzegane, 1987; Kienast et al., 1996; Ouzegane et al., 2003). By contrast to the Tassendjanet terrane, the In Ouzzal terrane has been largely preserved during the Pan-African orogeny, during which it behaved as a rigid body. It was only partly dissected by shear-zones and intruded by high-level granites at the end of the Pan-African convergence. The In Ouzzal terrane can be considered as a metacraton, which is a partially destabilised craton (Abdelsalam et al., 2002; Liégeois et al., 2003). This is a major point as it is the difference in rheological behaviour between the rigid In Ouzzal terrane and the more plastic Tassendjanet terrane that allowed the emplacement of the Tin Zebane complex (Hadj-Kaddour et al., 1998).

The Tin Zebane dyke complex (alkaline to peralkaline granites and tholeiitic gabbros) was indeed emplaced west of the In Ouzzal metacratonic terrane along the West-Ouzzalian shear zone (Dostal et al., 1979; Hadj-Kaddour et al., 1998). The studied Tin Zebane gabbro–anorthosite suite is associated with this dyke swarm. Most bodies are intruded, with sharp contacts, into the Pan-African high-pressure metamorphic rocks of the Tassendjanet terrane. They consist of kyanite–garnet bearing quartzites, garnet amphibolites and eclogites. Within this basement, the dominant planar structure is a penetrative foliation (F_1) defined by parallel alignments of muscovite and/or amphibole, depending on the nature of the host rock (quartzite, amphibolite). F_1 in quartzites is affected by folds (of decimetre to kilometre scale) with north–south subvertical striking and east or west dipping axial planes along the West-Ouzzalian shear zone. Fold axes plunge steeply (40°) to the north except in some shear zone localities where they show shallow to horizontal plunges. In most of the exposures, kyanite, garnet and muscovite are elongated or show sinistral rotation relative to the foliation. All these structures, related to thrusting and transpressive movements, are cross-cut by the Tin Zebane complex.

The Tin Zebane dyke complex is a 10 km wide dense swarm, without any screen of country-rocks. The alkaline peralkaline granites are relatively preserved from deformation in the central part of the dyke swarm but are deformed at the outer parts and become mylonitic within the West-Ouzzalian mylonitic shear zone. This swarm shows a large open sigmoidal fold. This feature is in agreement with opening tension gashes in a widening transtensional site (Caby, 1970; Hadj-Kaddour et al., 1998). The large-scale fold/gash is thus considered as syn- to late-magmatic and is probably connected with the large-scale sinistral displacement along the West Ouzzalian fault. Most felsic rocks were ductilely deformed and partially recrystallised under deep greenschist conditions. This recrystallisation occurred during and after the final consolidation of the magma and uplift of the complex (Hadj-Kaddour et al., 1998). The emplacement of the Tin Zebane magmatic complex is younger than all the transpressive movements responsible for the displacement of the Tuareg terranes (Black et al., 1994). It is followed by the brittle tectonics associated with small rift development associated with undeformed alkaline–peralkaline dyke swarms along the same shear zone (Dostal et al., 1979). The Tin Zebane magmatic complex marks the beginning of the transtensional movements along the shear zones, which correspond to the end of the post-collisional movements.

The Tin Zebane gabbroic suite forms a set of small lenticular to round-shaped bodies of 10–40 m in diameter. The exposed part of the intrusions is composed of coarse-grained rocks with a magmatic bedding plane

generally of millimetre to centimetre scale, layers of metre to ten metres scale are also observed. Layers are defined by variable proportions of plagioclase and olivine and can be then divided into three units: (1) anorthosite, (2) olivine-free gabbro/leucogabbro and, (3) olivine gabbro/leucogabbro. Massive gabbros–leucogabbros interlayered with anorthosites look undeformed, having preserved their magmatic structures, with the exception of the presence of coronitic textures. However, petrographical observations such as polygonal plagioclase and the chemistry out of equilibrium of the primary mineral phases will show this is not the case.

3. Petrography and mineral chemistry

All three groups contain plagioclase, magnetite and/or ilmenite. The anorthosite bears some amphibole. Clinopyroxene and orthopyroxene, in variable amounts, coexist with plagioclase in both gabbro/leucogabbro groups. Olivine gabbro/leucogabbro contains spinel in addition.

Magmatic minerals such as plagioclase, olivine and pyroxenes and cumulate textures are well preserved although a recrystallisation occurred (polygonal plagioclase). Some rocks show minerals in textural equilibrium, whereas some others e.g. olivine-gabbro display reactional, symplectitic intergrowths and coronas at the margins of the primary coarse grains.

Rocks completely retrogressed in the greenschist facies contain epidote–chlorite–actinolite–sericite replacing completely the primary minerals. Anorthosites show characteristic green patches of altered mafic minerals. Epidote often occurs at the plagioclase periphery in aggregates with chlorite and in plagioclase with muscovite and sericite. Amphibolite facies is never reached.

3.1. Anorthosites

The anorthosites (>90% plagioclase) show coarse-grained or polygonal textures (Fig. 3a) with medium grains (millimetre-scale, less than 1 cm) represented by subeuhedral or polygonal plagioclase ($An_{86–74}$) slightly zoned with higher An content in the cores (Fig. 4, Table 1). Amphibole occurs sometimes at the plagioclase crystal interfaces. It is a pargasite according to Leake et al. (1997) classification (Fig. 5A). Amphibole has relatively restricted X_{Mg} (0.74–0.77) and the sum (TiO_2 + Cr_2O_3 + MnO) is lower than 0.7 wt.% (Table 2).

3.2. Olivine-free gabbro to leucogabbro

In the olivine-free gabbro, coarse-grained commonly poekilitic heterogranular magmatic minerals include plagioclase, amphibole and locally clinopyroxene. Magnetite in small amount is the common oxide but rare ilmenite is present.

Plagioclase laths with interstitial subhedral amphibole define a magmatic layering characteristic of cumulative gabbros. Amphibole may contain numerous quartz and plagioclase inclusions of varied size and shape. In some samples, clinopyroxene is included in amphibole or forms large crystals coexisting with plagioclase, amphibole and magnetite.

Chemical analyses of minerals from the olivine-free gabbro show that plagioclase ($An_{86–73}$, bytownite) is slightly zoned with a core to rim enrichment in calcium, from An_{82} to An_{85} (Fig. 4). At the amphibole contact, plagioclase is generally enriched in sodium (An_{81}–An_{79}). The associated amphibole (X_{Mg} 0.69–0.89, Table 2) is a pargasite (Fig. 5C) and a magnesio-hornblende that extends to tschermakite (Fig. 5D). Actinolite is related to the latest stage of gabbro evolution, under greenschist facies. The amphibole TiO_2 content does not exceed 1.8 wt.% and Cr_2O_3 is low. The most magnesian amphibole is associated with rare clinopyroxene (Fig. 6A), which is a diopside ($En_{41–46}Fs_{05–09}Wo_{44–50}$) with X_{Mg} between 0.83 and 0.90 (Table 3). Al_2O_3 is up to 4.7 wt.% whereas Na_2O, Cr_2O_3, TiO_2 and Fe_2O_3 reach 0.6, 1.57, 0.56, and 3.37 wt.% respectively.

3.3. Olivine gabbro

3.3.1. General texture

The primary magmatic association is composed of olivine, clinopyroxene, plagioclase, minor orthopyroxene and oxides, i.e. magnetite locally with minute grains of spinel and ilmenite exsolutions. The rock is a coarse-grained heterogranular cumulate with individual grains ranging from millimetre to centimetre in long. The intercumulus material overgrowths cumulus grains. Highly cracked olivine displays embayments and generally include magnetite grains of variable size and shape, mainly along cracks, and some small rounded spinel grains (0.01–0.04 mm; Fig. 3c). Spinel is either primary, especially when coexisting with olivine, or an exsolution product when associated to magnetite. Large euhedral clinopyroxenes contain plagioclase inclusions and needles of magnetite.

Secondary minerals consist of amphibole, spinel, orthopyroxene, pigeonite and clinopyroxene. The reaction between olivine, pyroxene and plagioclase gives rise to amphibole coronas of variable thickness (<0.1–1 mm; Fig. 3b and c) locally associated to secondary orthopyroxene, clinopyroxene or pigeonite around olivine and pyroxene. Olivine is sometimes rimmed by a very fine symplectite of amphibole, spinel and drop-shaped orthopyroxene locally associated with clinopyroxene (Fig. 3c and d). The following reaction can then be proposed:

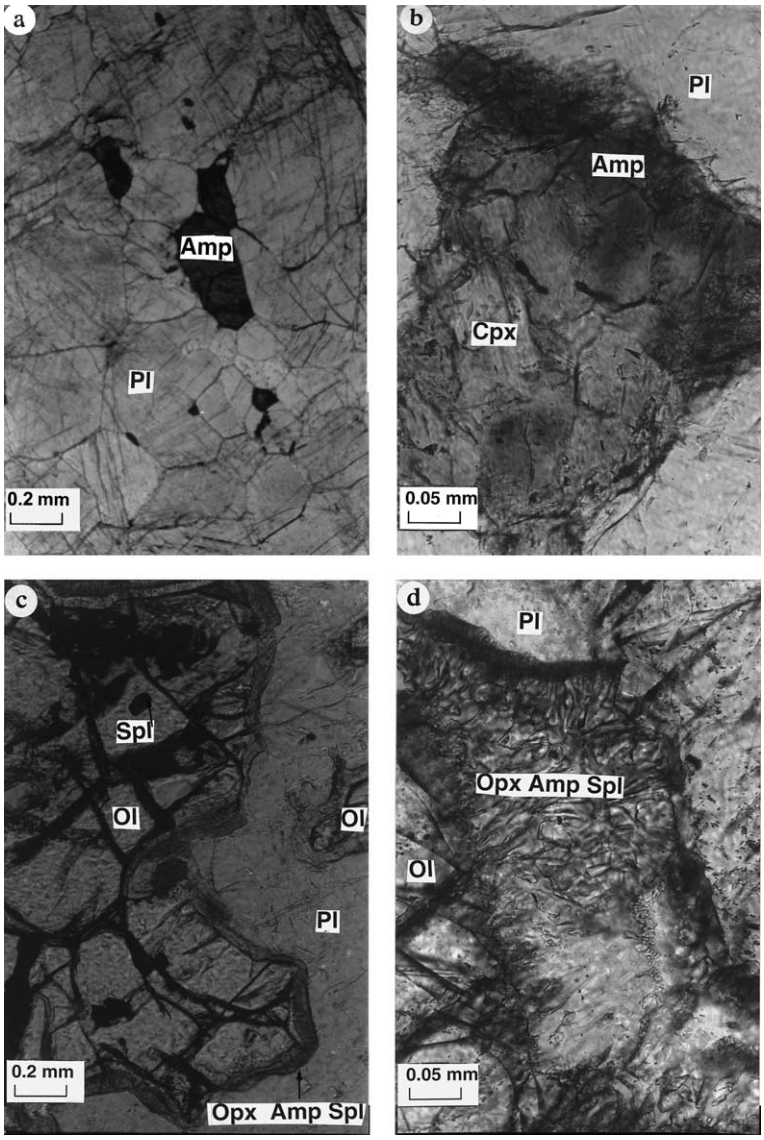

Fig. 3. Photomicrographs of thin section of anorthosite and gabbro from Tin Zebane. Abbreviations after Kretz (1983). (a) Granoblastic texture showing nearly polygonal mosaic of plagioclase associated with amphibole in anorthosite. (b) Amphibole mantling clinopyroxene in gabbro. (c) Coronas of amphibole–orthopyroxene–spinel, which have grown between olivine and plagioclase. Note also spinel included in olivine in gabbro. (d) Symplectites of orthopyroxene–amphibole and spinel at the boundary of olivine and plagioclase in gabbro.

$$\text{olivine} + \text{plagioclase} = \text{orthopyroxene} + \text{spinel} + \text{amphibole} \pm \text{clinopyroxene}.$$

3.3.2. Mineral compositions

Plagioclase ($An_{93–70}$) varies from bytownite to anorthite and shows an increasing anorthite content from the centre to the rim (Fig. 4) in contact with other minerals (olivine, clinopyroxene and amphibole).

Orthopyroxene ($X_{Mg} = 0.74–0.80$, $En_{73–78}$; Table 4) incorporates up to 3% wollastonite. Al_2O_3 can reach 2.8 wt.%; Na_2O does not exceed 2 wt.%; other elements are in low abundances. Primary orthopyroxene cores are slightly richer in magnesium than rims (Fig. 6B). Secondary orthopyroxene in corona reaction around clinopyroxene and olivine has variable composition: orthopyroxene associated with spinel around olivine is slightly lower in Mg ($\sim En_{75}$) than when developed between clinopyroxene and plagioclase ($\sim En_{77}$).

Clinopyroxene ($X_{Mg} = 0.77–0.90$) has up to 4.3 wt.% Al_2O_3. The maximum values of Na_2O, Fe_2O_3, TiO_2 and Cr_2O_3 are respectively 0.58, 3.25, 0.75 and 0.49 wt.%. Primary clinopyroxene ranges from diopside to augite ($En_{43–48}Fs_{05–13}Wo_{40–49}$; Fig. 6B). It is mainly zoned in Ca with core (about 48% wollastonite mole) Ca-richer than rims (down to 44% wollastonite mole). However, at the plagioclase contact, clinopyroxene shows a rapid

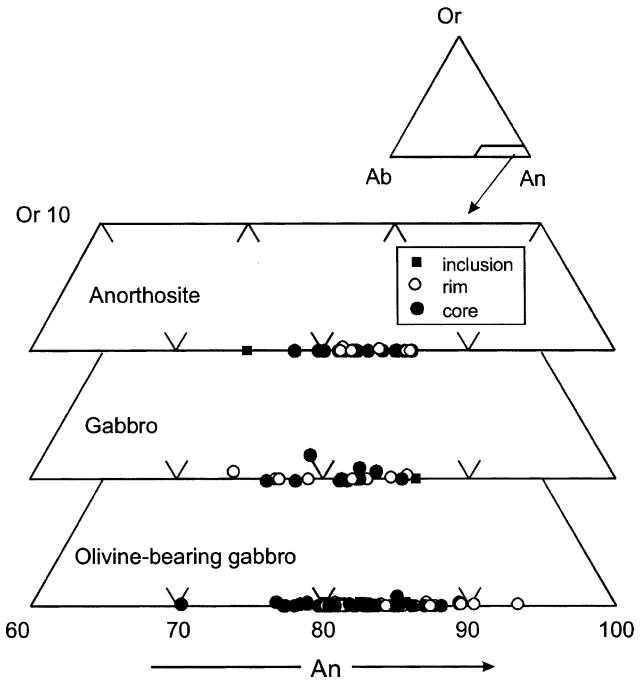

Fig. 4. Plagioclase compositions for the anorthositic gabbro, the gabbro and the olivine-gabbro.

increase in Ca (about 42–44% to 48% in mole of wollastonite). Secondary clinopyroxene occurs in corona with amphibole around orthopyroxene–clinopyroxene: this is a diopside $En_{44-46}Fs_{07-09}Wo_{48}$ when developed at the contact with primary orthopyroxene and a magnesian augite ($En_{61}Fs_{10}Wo_{29}$) when close to the external amphibole corona around the orthopyroxene. A magnesian pigeonite ($En_{70-75}Fs_{19-20}Wo_{6-10}$) is found in corona with secondary orthopyroxene around the primary clinopyroxene.

Olivine ($X_{Mg} = 0.71–0.78$, Table 5) contains only small amounts of MnO (less than 0.53 wt.%). Other elements are very low (<0.2 wt.% NiO, <0.1 wt.% Cr_2O_3 and CaO). However, numerous inclusions of magnetite and Cr-spinel indicate that olivine could have exsolved some Fe^{3+} and Cr. Olivine is nearly homogeneous although it is slightly enriched in Mg at the contact of pyroxenes and amphibole.

Spinel has a variable composition ($X_{Mg} = 0.34–0.57$, Table 6): it is a solid solution between hercynite and spinel with low TiO_2 and ZnO contents (<1 wt.%). Secondary spinel ($X_{Mg} = 0.48–0.52$) is relatively magnesian. Primary spinel from the same sample (TZ134) is the most ferriferous ($X_{Mg} = 0.34–0.37$) and the least aluminous and is rich in chromium (Cr_2O_3 up to 13 wt.%). The latter is associated with the most magnesian olivine ($X_{Mg} = 0.76–0.77$ in TZ134) whereas the least magnesian olivine ($X_{Mg} = 0.71–0.73$ in TZ30) is

Table 1
Representative chemical compositions of the Tin Zebane anorthositic gabbro minerals[a]: plagioclase, structural formulae based on 8 oxygen atoms; all iron is ferrous

Rock	Anorthosite				Gabbro		Olivine bearing gabbro									
Sample	TZ144	TZ123	TZ123	TZ123	TZ124	TZ146	TZ124	TZ124	TZ124	TZ30	TZ30	TZ30	TZ30	TZ134	TZ30	TZ30
Analysis	51	63	65	67	30	31	29	34	24	121	38	3	30	104	37	48
Remarks	Core	Core	Rim	Rim	Core	Core	Rim	Rim	Inclusion	Core	Core	Rim	Rim	Rim	Inclusion	Inclusion
SiO_2	48.49	46.19	46.04	46.32	47.41	47.57	46.82	47.76	47.22	50.39	45.52	49.05	47.26	47.47	47.98	46.68
Al_2O_3	32.89	33.76	34.19	32.89	34.00	33.05	34.07	32.62	33.99	32.04	29.44	32.84	34.14	33.73	33.47	34.30
FeO	0.10	0.00	0.00	0.00	0.05	0.14	0.20	0.10	0.04	0.13	3.12	0.02	0.23	0.19	0.28	0.35
CaO	16.34	17.23	17.28	16.86	17.84	16.33	17.64	15.72	18.32	13.25	15.12	15.78	16.96	16.07	16.24	17.11
Na_2O	2.30	1.55	1.58	2.05	1.70	2.09	1.61	3.05	1.61	3.10	1.76	2.33	1.85	1.87	2.23	1.58
K_2O	0.00	0.00	0.00	0.00	0.01	0.01	0.04	0.12	0.03	0.02	0.05	0.04	0.02	0.00	0.04	0.06
TOTAL	100.17	98.75	99.16	98.21	101.03	99.27	100.52	99.58	101.26	99.16	99.29	100.23	100.45	99.57	100.30	100.17
Structural formulae on 8 oxygens																
Si	2.217	2.148	2.134	2.168	2.158	2.196	2.144	2.204	2.148	2.304	2.143	2.235	2.160	2.182	2.193	2.142
Al	1.772	1.850	1.867	1.814	1.824	1.798	1.839	1.774	1.823	1.727	1.633	1.764	1.839	1.827	1.803	1.855
Fe	0.004	0.000	0.000	0.000	0.002	0.005	0.008	0.004	0.002	0.005	0.123	0.001	0.009	0.007	0.011	0.013
Ca	0.800	0.858	0.858	0.845	0.870	0.808	0.866	0.777	0.893	0.649	0.763	0.770	0.831	0.791	0.795	0.841
Na	0.204	0.139	0.142	0.186	0.150	0.187	0.143	0.273	0.142	0.275	0.160	0.206	0.164	0.167	0.198	0.140
K	0.000	0.000	0.000	0.000	0.001	0.001	0.002	0.007	0.002	0.001	0.003	0.002	0.001	0.000	0.002	0.003
Sum	4.997	4.996	5.001	5.013	5.005	4.995	5.002	5.039	5.010	4.961	4.825	4.978	5.003	4.975	5.002	4.996
%An	79.67	86.02	85.79	81.94	85.21	81.10	85.63	73.54	86.13	70.16	82.36	78.74	83.45	82.61	79.91	85.42
%Ab	20.33	13.98	14.22	18.06	14.71	18.82	14.13	25.81	13.70	29.70	17.32	21.03	16.44	17.39	19.86	14.24
%Or	0.00	0.00	0.00	0.00	0.07	0.08	0.24	0.65	0.17	0.14	0.33	0.23	0.11	0.00	0.22	0.35

[a] The compositional variation of minerals was determined using a Cameca SX50 electron microprobe at the University of Paris VI. The operating conditions included an accelerating voltage of 15 kV and a sample current of 10 nA. Natural minerals and synthetic oxides were used as standards for all elements except for fluorine and zinc that were, respectively calibrated on fluorite and sphalerite.

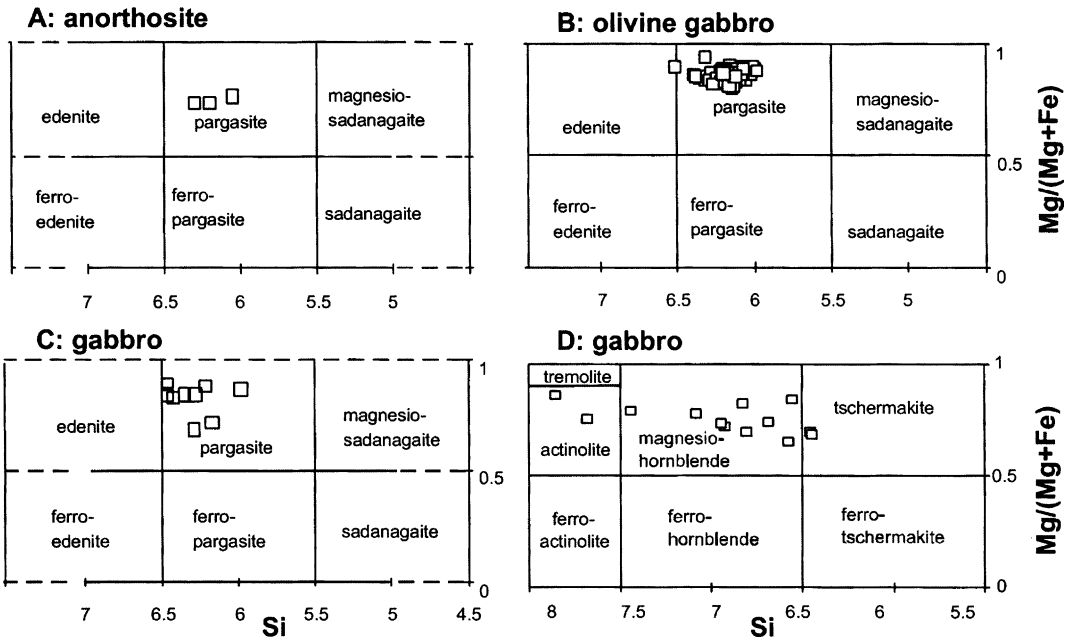

Fig. 5. Ca-amphibole compositions for samples from the Tin Zebane anorthositic gabbro. Diagram parameters are (A), (B), (C) $Ca_B \geqslant 1.50$; $(Na + K)_A \geqslant 0.50$; $Ti < 0.50$ and (D) $Ca_B \geqslant 1.50$; $(Na + K)_A \leqslant 0.50$ (after Leake et al., 1997).

Table 2
See Table 1 caption and the footnote in that table; amphibole, structural formulae based on 22 oxygen atoms (and 2OH); Ferric iron after Holland and Blundy (1994)

Rock	Anorthosite	Gabbro					Olivine bearing gabbro		
Sample	TZ144	TZ146	TZ124	TZ137	TZ124	TZ116	TZ134	TZ134	TZ134
Analysis	49	24	27	33	28	16	164	170	180
Remarks		Core	Core	Core	Rim	Rim	Corona	Corona	Corona
SiO_2	42.32	42.52	48.91	43.74	45.71	45.20	42.55	43.42	44.32
TiO_2	0.15	1.78	0.49	0.24	0.64	1.07	0.05	1.83	0.54
Al_2O_3	15.30	12.71	9.78	14.65	14.12	12.55	16.23	14.29	12.42
Cr_2O_3	0.00	0.02	0.00	0.01	0.00	0.50	0.00	0.21	0.16
NiO	0.02	0.00	0.00	0.00	0.06	0.00	0.03	0.07	0.05
MgO	10.98	11.04	14.10	15.39	11.56	16.31	12.68	15.06	18.21
FeO	13.81	14.24	11.90	8.52	12.14	6.98	10.37	8.43	7.35
MnO	0.33	0.27	0.04	0.09	0.05	0.25	0.18	0.10	0.08
CaO	10.85	11.47	12.70	12.29	12.21	11.33	11.85	11.67	10.76
Na_2O	2.03	1.49	1.00	2.51	1.27	1.82	2.35	2.08	1.98
K_2O	0.17	0.39	0.18	0.12	0.32	0.27	0.19	0.34	0.14
H_2O	1.95	1.97	2.09	2.08	2.00	2.03	2.03	2.07	2.05
F	0.11	0.00	0.03	0.00	0.13	0.00	0.00	0.01	0.01
Cl	0.00	0.07	0.00	0.01	0.05	0.19	0.03	0.02	0.04
Sum	98.01	97.96	101.20	99.64	100.28	98.50	98.56	99.59	98.10
Si	6.211	6.304	6.926	6.222	6.579	6.469	6.158	6.194	6.337
Ti	0.017	0.198	0.052	0.026	0.069	0.115	0.006	0.196	0.058
Al	2.647	2.220	1.633	2.456	2.396	2.118	2.768	2.402	2.094
Cr	0.000	0.002	0.000	0.001	0.000	0.057	0.000	0.023	0.018
Fe3	0.847	0.698	0.252	0.603	0.127	0.418	0.628	0.503	0.665
Ni	0.002	0.000	0.000	0.000	0.007	0.000	0.004	0.008	0.006
Mg	2.401	2.440	2.976	3.263	2.481	3.479	2.736	3.201	3.882
Fe_2	0.847	1.067	1.156	0.411	1.335	0.418	0.628	0.503	0.214
Mn	0.042	0.033	0.005	0.011	0.006	0.030	0.022	0.013	0.009
Ca	1.706	1.822	1.927	1.874	1.883	1.738	1.839	1.783	1.649
Na	0.576	0.427	0.273	0.691	0.356	0.506	0.660	0.576	0.548
K	0.032	0.074	0.032	0.022	0.059	0.049	0.035	0.061	0.026
Sum	15.329	15.287	15.232	15.579	15.298	15.396	15.485	15.464	15.504
X_{Mg}	0.74	0.70	0.72	0.89	0.65	0.89	0.81	0.86	0.95

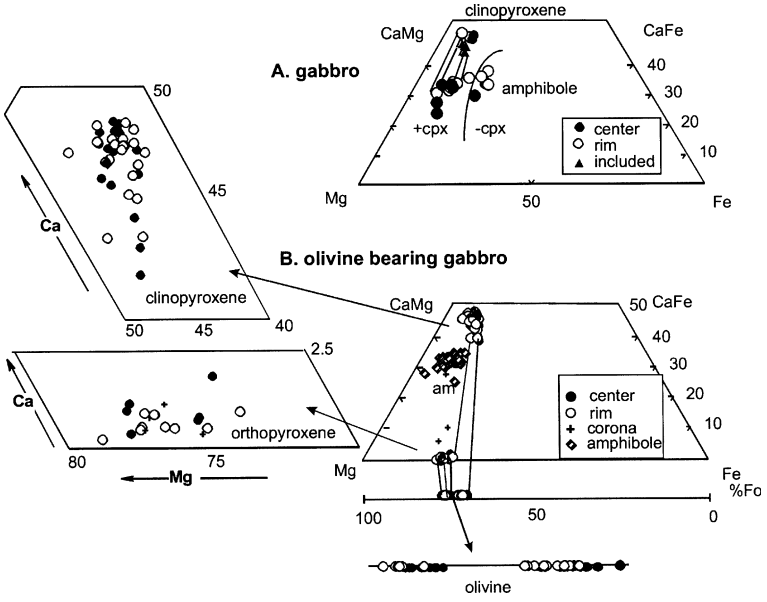

Fig. 6. Compositions of Fe–Mg–minerals plotted in the pyroxene quadrilateral for (A) the gabbro, (B) the olivine-gabbro.

Table 3
See Table 1 caption and the footnote in that table; clinopyroxene, structural formulae based on 6 oxygen atoms and 4 cations

Rock	Gabbro Clinopyroxene						Olivine bearing gabbro Clinopyroxene–pigeonite							
Sample	TZ137	TZ137	TZ137	TZ137	TZ116	TZ116	TZ30	TZ30	TZ30	TZ145	TZ30	TZ30	TZ134	TZ30
Analysis	20	22	23	19	3	7	1	27	29	18	66	57	161	43
Remarks	Core	Core	Rim	Rim	Inclu-sion	Inclu-sion	Co-rona[a]	Core	Core	Core	Rim	Rim	Rim	Rim
SiO_2	52.49	50.90	50.82	51.57	49.94	54.53	57.92	52.05	51.33	51.22	51.53	51.00	55.00	52.25
TiO_2	0.18	0.41	0.42	0.33	0.56	0.55	0.12	0.69	0.73	0.00	0.20	0.64	0.29	0.28
Al_2O_3	2.19	3.40	3.19	2.96	4.67	1.29	1.45	3.06	2.98	3.29	4.34	2.50	2.68	2.70
Cr_2O_3	0.23	0.32	0.20	0.17	1.57	0.44	0.00	0.34	0.36	0.23	0.26	0.48	0.39	0.21
Fe_2O_3	0.00	1.17	3.37	2.03	1.51	0.00	0.00	0.00	2.52	1.53	2.49	0.91	0.00	1.90
MgO	14.09	13.97	14.65	14.30	15.03	16.13	23.54	15.89	15.08	14.53	15.68	15.44	20.22	15.29
FeO	4.94	5.06	2.92	4.62	5.00	4.21	11.77	8.02	3.92	4.15	3.17	7.81	5.96	3.74
MnO	0.18	0.29	0.31	0.24	0.00	0.42	0.38	0.34	0.30	0.09	0.19	0.09	0.17	0.25
CaO	23.77	22.71	23.43	23.16	19.94	23.02	5.03	19.11	22.80	22.97	21.69	19.19	13.07	23.39
Na_2O	0.42	0.40	0.35	0.37	0.59	0.36	0.17	0.36	0.34	0.36	0.58	0.33	0.27	0.33
Sum	98.49	98.63	99.66	99.75	98.81	100.95	100.38	99.86	100.36	98.37	100.13	98.39	98.07	100.34
Si	1.960	1.907	1.882	1.910	1.860	1.975	2.051	1.922	1.888	1.916	1.884	1.919	1.998	1.916
Ti	0.005	0.012	0.012	0.009	0.016	0.015	0.003	0.019	0.020	0.000	0.006	0.018	0.008	0.008
Al	0.096	0.150	0.139	0.129	0.205	0.055	0.061	0.133	0.129	0.145	0.187	0.111	0.115	0.117
Cr	0.007	0.009	0.006	0.005	0.046	0.013	0.000	0.010	0.010	0.007	0.007	0.014	0.011	0.006
Fe_3	0.000	0.033	0.094	0.056	0.042	0.000	0.000	0.000	0.070	0.043	0.069	0.026	0.000	0.053
Mg	0.784	0.780	0.809	0.790	0.835	0.871	1.243	0.875	0.827	0.810	0.854	0.866	1.095	0.836
Fe_2	0.154	0.158	0.091	0.143	0.156	0.127	0.349	0.248	0.121	0.130	0.097	0.246	0.181	0.115
Mn	0.006	0.009	0.010	0.008	0.000	0.013	0.011	0.011	0.009	0.003	0.006	0.003	0.005	0.008
Ca	0.951	0.911	0.930	0.919	0.796	0.894	0.191	0.756	0.898	0.921	0.850	0.774	0.509	0.919
Na	0.030	0.029	0.025	0.026	0.043	0.025	0.012	0.025	0.025	0.026	0.041	0.024	0.020	0.023
Sum	3.993	3.998	3.998	3.995	3.999	3.988	3.921	3.999	3.997	4.001	4.001	4.001	3.942	4.001
X_{Mg}	0.84	0.83	0.90	0.85	0.84	0.87	0.78	0.78	0.87	0.86	0.90	0.78	0.86	0.88

[a] Pigeonite.

associated with the more magnesian spinel (X_{Mg} = 0.46–0.57).

Amphibole (X_{Mg} = 0.81–0.95, Table 2) is a pargasite and one analysis corresponds to an edenite according to

Table 4
See Table 1 caption and the footnote in that table; orthopyroxene, structural formulae based on 6 oxygen atoms and 4 cations

Rock	Olivine bearing gabbro Orthopyroxene						
Sample	TZ134	TZ145	TZ30	TZ30	TZ30	TZ30	TZ30
Analysis	162	4	48	131	14	60	71
Remarks	Rim	Rim	Core	Core	Corona	Corona	Corona
SiO_2	53.72	54.34	54.18	53.51	53.90	56.09	53.02
TiO_2	0.35	0.08	0.05	0.14	0.02	0.01	0.00
Al_2O_3	1.68	2.83	1.70	1.71	2.39	0.89	2.39
Cr_2O_3	0.14	0.00	0.06	0.08	0.14	0.00	0.00
Fe_2O_3	0.25	0.56	0.00	1.19	0.63	0.00	1.73
MgO	26.44	28.42	26.67	27.68	26.87	26.08	27.35
FeO	16.14	13.50	15.09	13.50	15.51	11.60	13.79
MnO	0.34	0.47	0.43	0.31	0.49	0.28	0.41
CaO	0.73	0.17	0.61	0.74	0.27	3.07	0.26
Na_2O	0.00	0.00	0.06	0.00	0.02	0.08	0.02
Sum	99.79	100.37	98.85	98.86	100.24	98.10	98.97
Si	1.949	1.932	1.969	1.942	1.939	2.028	1.926
Ti	0.010	0.002	0.001	0.004	0.000	0.000	0.000
Al	0.072	0.118	0.073	0.073	0.101	0.038	0.102
Cr	0.004	0.000	0.002	0.002	0.004	0.000	0.000
Fe_3	0.007	0.015	0.000	0.033	0.017	0.000	0.047
Mg	1.430	1.507	1.445	1.498	1.441	1.405	1.481
Fe_2	0.490	0.401	0.459	0.410	0.467	0.351	0.419
Mn	0.010	0.014	0.013	0.010	0.015	0.009	0.013
Ca	0.028	0.007	0.024	0.029	0.010	0.119	0.010
Na	0.000	0.000	0.004	0.000	0.002	0.006	0.001
Sum	4.000	3.996	3.990	4.001	3.996	3.956	3.999
X_{Mg}	0.74	0.79	0.76	0.79	0.76	0.80	0.78

Leake et al. (1997, Fig. 5B) Al_2O_3 ranges from 11.9 to 16.8 wt.%; TiO_2 does not exceed 2 wt.%, Cr_2O_3 0.75 wt.% and MnO 0.4 wt.%.

3.3.3. Pressure–temperature conditions for symplectites and coronas formation

The textural relations in the olivine gabbro allow distinguishing two successive mineral associations: (1) a primary association composed of olivine, clinopyroxene, orthopyroxene and plagioclase; (2) a secondary association consisting in coronas of amphibole, ±pigeonite, ±clinopyroxene, ±orthopyroxene and in symplectites of amphibole, orthopyroxene, clinopyroxene and spinel that result from reactions between olivine and plagioclase.

The P–T–a_{H2O} conditions were calculated using Thermocalc (Holland and Powell, 1998). Pressure–temperature estimations gave meaningful results only for the secondary mineral assemblage, the primary minerals appearing to be in disequilibrium. The average pressure–temperature was determined for the secondary assemblage using olivine–plagioclase rim compositions with secondary pigeonite–orthopyroxene–spinel–amphibole compositions from symplectites and coronas. A set of independent reactions between end-members was used to estimate the pressure and the temperature in dependence with a_{H2O} as amphibole is a hydrous mineral. Pressure, temperature and a_{H2O} values were accepted if the fit test was passed. The values with a good fit are around 800 °C (797 ± 42 °C for $a_{H2O} = 0.5$ and 808 ± 44 °C for

Table 5
See Table 1 caption and the footnote in that table; olivine, structural formulae based on 4 oxygen atoms

Rock	Olivine bearing gabbro Olivine			
Sample	TZ30	TZ145	TZ30	TZ134
Analysis	47	5	72	102
Remarks	Core	Core	Rim	Rim
SiO_2	36.82	38.37	37.09	38.30
TiO_2	0.00	0.01	0.00	0.00
NiO	0.00	0.06	0.07	0.05
MgO	36.82	39.35	36.56	40.03
FeO	26.12	21.89	25.61	21.37
MnO	0.38	0.27	0.48	0.24
CaO	0.00	0.03	0.10	0.00
Sum	100.14	99.98	99.91	99.99
Si	0.977	0.996	0.985	0.992
Cr	0.000	0.000	0.000	0.000
Ni	0.000	0.001	0.001	0.001
Mg	1.457	1.523	1.447	1.546
Fe_2	0.580	0.475	0.569	0.463
Mn	0.009	0.006	0.011	0.005
Ca	0.000	0.001	0.003	0.000
Sum	3.023	3.004	3.016	3.008
X_{Mg}	0.72	0.76	0.72	0.77

Table 6
See Table 1 caption and the footnote in that table; oxides, spinel and magnetite structural formulae based on 32 oxygen atoms and 24 cations; ilmenite structural formulae based on 3 oxygen atoms and 2 cations

Rock	Olivine bearing gabbro										
	Magnetite			Ilmenite	Spinel						
Sample	TZ30	TZ30	TZ30	TZ134	TZ30	TZ30	TZ30	TZ134	TZ134	TZ30	TZ30
Analysis	22	117	127	96	7	85	80	106	113	41	87
Remarks					Inclusion	Inclusion	Corona	Inclusion	Corona	Corona	Corona
SiO_2	0.05	0.08	0.03	0.00	0.05	0.09	0.29	0.80	0.01	0.09	0.01
TiO_2	0.37	5.57	0.27	49.13	0.04	0.05	0.02	0.03	0.33	0.02	0.03
Al_2O_3	0.61	2.81	0.51	0.01	62.39	59.72	62.49	48.94	44.85	60.34	60.13
Cr_2O_3	3.51	2.23	2.30	0.48	0.03	2.82	0.00	9.81	12.94	2.73	2.02
Fe_2O_3	63.90	52.49	64.86	7.77	3.28	2.62	1.45	4.10	7.53	0.67	3.54
NiO	0.06	0.09	0.00	0.12	0.14	0.25	0.15	0.17	0.23	0.20	0.20
MgO	0.09	0.69	0.21	2.43	14.02	12.87	12.28	7.87	8.33	11.21	13.15
FeO	31.13	35.30	30.70	37.85	19.06	21.19	22.56	27.61	25.81	23.84	20.77
MnO	0.09	0.21	0.06	1.46	0.27	0.09	0.10	0.39	0.28	0.21	0.19
ZnO	0.09	0.00	0.00	0.04	1.00	0.26	0.29	0.48	0.49	0.00	0.35
CaO	0.08	0.02	0.00	0.18	0.09	0.07	0.15	0.22	0.00	0.04	0.07
Sum	99.97	99.48	98.94	99.50	100.41	100.04	99.83	100.42	100.83	99.44	100.46
Si	0.016	0.024	0.008	0.000	0.008	0.016	0.064	0.184	0.000	0.016	0.000
Ti	0.088	1.264	0.064	0.923	0.008	0.008	0.000	0.008	0.056	0.000	0.008
Al	0.216	1.000	0.184	0.000	15.456	15.056	15.656	13.160	12.216	15.384	15.080
Cr	0.848	0.528	0.560	0.009	0.008	0.480	0.000	1.768	2.368	0.464	0.336
Fe_3	14.728	11.904	15.112	0.146	0.520	0.424	0.232	0.704	1.312	0.112	0.568
Ni	0.016	0.024	0.000	0.002	0.024	0.040	0.024	0.032	0.040	0.032	0.032
Mg	0.040	0.312	0.096	0.090	4.392	4.104	3.888	2.680	2.872	3.616	4.168
Fe_2	7.976	8.896	7.952	0.791	3.352	3.792	4.008	5.264	4.992	4.312	3.696
Mn	0.024	0.056	0.016	0.031	0.048	0.016	0.016	0.072	0.056	0.040	0.032
Zn	0.024	0.000	0.000	0.001	0.152	0.040	0.048	0.080	0.080	0.000	0.056
Ca	0.024	0.008	0.000	0.005	0.016	0.016	0.032	0.056	0.000	0.008	0.016
Sum	24.00	24.00	24.00	2.00	24.00	24.00	24.00	24.00	24.00	24.02	24.00
X_{Mg}	–	–	–	–	0.57	0.52	0.49	0.34	0.37	0.46	0.53

$a_{H2O} = 0.6$) and 6.2 ± 1.4 kbar for a_{H2O} ranging between 0.5 and 0.6. Detailed results are given in Table 7.

A main question concerning these coronitic and symplectitic textures is to know if they are magmatic and formed during the cooling of the gabbroic body or metamorphic, i.e. related to a subsequent event. In the first case, the mass transfer to be envisaged is between olivine, plagioclase and an intergranular fluid and in the second case only between olivine and plagioclase. Most authors (e.g. Ashworth, 1986 and references therein) consider that coronas have originated through a metamorphic reaction between plagioclase and olivine because: (1) they always occur where olivine and plagioclase are adjacent and never between olivine and augite; (2) the coronitic gabbro occur in amphibolite-facies and granulite-facies metamorphic terranes. For other authors (e.g. Joesten, 1986 and references therein), coronas can be also produced during the cooling of intrusions by reaction between olivine and liquid at high pressure, particularly in spinel-saturated basaltic magmas. Indeed, Joesten (1986) argued that magmas which crystallise from troctolite on the plagioclase–olivine cotectic at pressures below ~5 kbar form coronites at pressures greater than 5 kbar.

The pressure determined for the Tin Zebane gabbros (6.2 ± 1.4 kbar) is compatible with both models. Additional observations supporting the late magmatic origin include: (1) olivine is not systematically surrounded by spinel–orthopyroxene–amphibole symplectites; this is the case only for the most magnesian olivine usually associated with magnetite; this is more easily explained by the greater disequilibrium between this Mg-olivine with the residual liquid than in subsolidus metamorphic conditions. (2) Pargasitic amphibole in corona reflects high-temperature conditions (calculated temperature of 800 °C) again more easily compatible with a melt still remaining in the rocks. (3) The very small size of the dropped symplectites indicates a very rapid cooling of the magma, which quickly decreased the element mobility and stopped the diffusion of elements. (4) The gabbros show no mineral indicators of a high-pressure metamorphism such as garnet. (5) The Tin Zebane complex was emplaced in a big tension gash (Hadj-Kaddour et al., 1998) younger than the high-pressure metamorphism recorded in the eclogites (13–15 kbar; Caby and Monié, 2003).

The Tin Zebane gabbroic rocks are interpreted as free from post-magmatic metamorphic recrystallisation,

Table 7
Pressure–temperature–a_{H2O} calculations

Mineral	End member	Activity (a)	sd(a)/a	$a_{(H2O)}$	T (°C)	sd(T)	P (kbar)	sd(P)	Fit (<1.45)
Pigeonite	di	0.710	0.05	0.5	797	42	6.2	1.4	1.41
	hed	0.170	0.21	0.6	808	44	6.2	1.4	1.43
	cats	0.084	0.25	0.7	817	45	6.3	1.5	1.45
Olivine	fo	0.560	0.10						
	fa	0.113	0.26						
Orthopyroxene	en	0.520	0.07						
	fs	0.059	0.34						
	mgts	0.031	0.32						
Plagioclase	an	0.880	0.05						
	ab	0.130	0.69						
Amphibole	tr	0.149	0.26						
	parg	0.415	0.21						
Spinel	sp	0.450	0.09						
	herc	0.530	0.07						

a = activity of end member in mineral, sd(a)/a = uncertainty.

except the late greenschist facies. They are made up of cumulus and intercumulus minerals but most of the grains grew together to form an aggregate by crystallisation from or reaction with trapped intercumulus liquid. The corona and symplectites represent the adjustment of the mineral assemblages to the dropping temperature during the cooling stage, which occurred at ca. 6.2 kbar/800 °C.

4. Strontium and neodymium isotopes: an uncontaminated OIB-type depleted mantle source

Sr and Nd isotope analyses were carried out at the Isotope Geology Laboratory of the Africa Museum in Tervuren (Belgium). The samples were dissolved into a suboiled HF–HNO_3 acid mixture; if a solid phase remained after centrifugation, they were again dissolved into the same acid mixture but into teflon-lined stainless-steel digestion vessels at 180 °C. Sr and Nd were separated on SPEC© ion-exchange resins following a procedure adapted from Pin et al. (1994). Sr isotopic compositions were measured on single Ta filament and Nd isotopic compositions on triple Ta–Re–Ta filament using a Micromass Sector 54 multi-collector mass spectrometer. Repeated measurements of Sr and Nd standards indicate that between-run error is better than ±0.000015. On each turret, four standards are measured together with 16 samples. The mean of the four standards was used to correct the bias relatively to recommended values (0.710250 for NBS987 and 0.511963 for Rennes standard, corresponding to a La Jolla standard value of 0.511858). During this study, NBS987 standard yielded a value for $^{87}Sr/^{86}Sr$ (normalised to $^{86}Sr/^{88}Sr = 0.1194$) of 0.710274 ± 0.000008 (mean on 4 standards), and the Rennes Nd standard $^{143}Nd/^{144}Nd$, a value (normalised to $^{146}Nd/^{144}Nd = 0.7219$) of 0.511965 ± 6 (on 4 standards). Rb and Sr concentrations were measured by X-ray fluorescence. The error on the Rb/Sr and Sm/Nd ratios is <4%. The Rb–Sr and Sm–Nd ages were calculated following Ludwig (1999). Used decay constants are 1.42×10^{-11} a^{-1} (^{87}Rb) and 6.54×10^{-12} a^{-1} (^{147}Sm). Results are given in Table 8.

The Tin Zebane gabbros and anorthosites have nearly no Rb and measured isotopic ratios are then very close to initial ratios. The latter are therefore known with a high reliability since error on age or on Rb/Sr ratio is of no influence. At 592 Ma (Rb–Sr isochron age on 19 Tin Zebane granitoids; Hadj-Kaddour et al., 1998), initial ratios of Tin Zebane mafic rocks (including anorthosite) vary within a very restricted range: initial $^{87}Sr/^{87}Sr$ (Sr_i) = 0.70257–0.70278 and $\varepsilon_{Nd} = +5.9$ to +7.8 (Fig. 7). T_{DM} model ages are close to the emplacement age, varying from 500 to 720 Ma. These parameters correspond to those of the Tin Zebane alkaline–peralkaline granitoids (including two gabbros; Hadj-Kaddour et al., 1998): $Sr_i = 0.70281 \pm 0.00001$ and $\varepsilon_{Nd} = +6.4 \pm 0.6$ (Fig. 7). In the Tuareg shield, such depleted mantle values are rare and only known in some Neoproterozoic island arc igneous suites formed before collision with the West African craton (Caby et al., 1989). The Tin Zebane complex is the only known intracontinental Tuareg magmatism displaying such isotopic characteristics. Considering this particular isotopic signature in continental regions as well as the close spatial relationships between the studied anorthosite and gabbros and the alkaline–peralkaline granitoid dyke swarm associated with large amounts of mafic rocks (although generally heavily retrograded) studied by Hadj-Kaddour et al. (1998), there is little doubt that

Table 8
Nd and Sr isotopic results

	Rb	Sr	$^{87}Rb/^{86}Sr$	$^{87}Sr/^{86}Sr$	2σ	Sr_i 592 Ma		
TZ30	0.83	322	0.007	0.702668	0.000011	0.702605		
TZ115	1.99	480	0.012	0.702880	0.000010	0.702779		
TZ123	2.03	521	0.011	0.702698	0.000008	0.702603		
TZ145	0.5	356	0.004	0.702604	0.000008	0.702570		
	Sm	Nd	$^{147}Sm/^{144}Nd$	$^{143}Nd/^{144}Nd$	2σ	$\varepsilon_{Nd(0\ Ma)}$	$\varepsilon_{Nd(592\ Ma)}$	T_{DM}
TZ30	0.36	1.1	0.1996	0.512963	0.000016	6.34	6.13	–
TZ115	0.6	2.26	0.1592	0.512793	0.000009	3.02	5.87	720
TZ123	0.31	1.38	0.1354	0.512798	0.000007	3.12	7.77	503
TZ145	0.3	1.23	0.1465	0.512770	0.000010	2.57	6.38	641

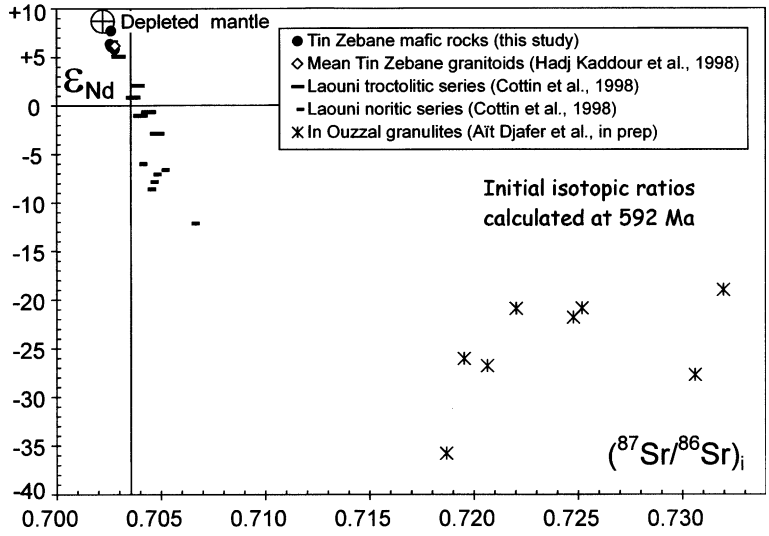

Fig. 7. Sr–Nd isotopes of the Tin Zebane gabbroic intrusions compared to the Laouni layered mafic–ultramafic intrusions (Cottin et al., 1998) and isotopic composition at 592 Ma of granulitic rocks from Archaean In Ouzzal metacratonic terrane (Aït-Djafer et al., 2003).

they belong to the same complex and that they are co-genetic. This supports the use of the age of the Tin Zebane granitoids (592.2 ± 5.8 Ma, 19 whole-rock Rb–Sr isochron; Hadj-Kaddour et al., 1998) for the studied mafic rocks. This implies also that all the rocks from the Tin Zebane complex, from gabbros to granites, share the same source, i.e. an OIB-type depleted mantle corresponding to the "prevalent mantle" (PREMA, Zindler and Hart, 1986), as shown by Hadj-Kaddour et al. (1998). Indeed, these authors showed that both Sr and Nd isotopic ratios of the Tin Zebane granitoids correspond closely to the PREMA isotopic composition at ca. 592 Ma. The absence of crystal contamination is well constrained within the Tin Zebane complex as the country-rocks are much older (ca. 2 Ga or Archaean) and are then in strong isotopic contrast with the Pan-African mantle. This can be shown by using the Sr–Nd isotopic compositions of granulitic rocks from In Ouzzal terrane, 25 km to the east of Tin Zebane (Tikechitine area; Aït-Djafer et al., 2003) as a reference (Fig. 7). At 592 Ma, their Sr_i are between 0.717 and 0.732 and their ε_{Nd} between −20 and −36. Even a slight contamination by such rocks would have been recorded by the Tin Zebane rocks.

Parallels can be drawn between the Tin Zebane gabbroic cumulates and the Laouni troctolitic–noritic layered intrusions in the Latea metacraton (Liégeois et al., 2003; Fig. 1) as they both are post-collisional and have similar petrographic features (Cottin et al., 1998). The Laouni cumulate piles are linked to two magmatic liquid lines of descent, one tholeiitic (troctolitic cumulates) and the other calc-alkaline (noritic cumulates), the second being more contaminated by continental crust (Fig. 7; Cottin et al., 1998). The comparison will be done mainly with the troctolitic series. The least contaminated sample from Laouni troctolitic series (2H669) has Sr and Nd initial isotopic ratios close to that of Tin Zebane gabbros: $\varepsilon_{Nd} = +5.9$, $(^{87}Sr/^{86}Sr)_i = Sr_i = 0.70297$ (Cottin et al., 1998). The mafic rocks studied here strengthen the hypothesis of a similar depleted mantle source in the Tin

Zebane and Laouni complexes, with an additional and variable crustal contamination only in the Laouni case (Cottin et al., 1998). This indicates that the Tin Zebane complex has counterparts in the Central Hoggar and this has general implications discussed later.

5. Geochemistry: plagioclase–pyroxenes–olivine cumulates

Care was taken to sample the freshest samples. Five samples were analysed for major, trace and REE element. Major elements were analysed by ICP-AES (total iron is reported as Fe_2O_3) and trace and other elements by ICP-MS at the CRPG laboratory of Nancy. Analytical uncertainties are better than 10%. Compositions of the Tin Zebane gabbros and anorthosite are given in Table 9. Two gabbros (samples HK188.2 and HK533) from the southern part of the Tin Zebane complex (Hadj-Kaddour et al., 1998) have been added for comparison.

The Tin Zebane samples are slightly silica-undersaturated especially the anorthosite, the cation normative feldspar content (An + Ab + Or) ranges from 58% to 91.4%, whereas the range of normative olivine lies between 1% in anorthosite and 12–27% in gabbros (Table 9). Gabbros HK188.2 and HK533 have higher SiO_2 (around 47%) than the other gabbroic rocks (43–45% SiO_2). This can be related to the alkali content: $Na_2O + K_2O$ range in the latter from 1.22% to 2.08% (with $K_2O < 0.1\%$), and reach 3.32% in samples HK188.2 and HK533 (Table 9).

The rocks show significant variations in Al_2O_3, MgO, FeO_t, and CaO content, which are mostly related to the amount of modal plagioclase against modal olivine and pyroxenes. The cumulates HK188.2 and HK533 have the highest TiO_2, FeO_t, MnO and Na_2O. The highest MgO content (11.6%) occurs in the olivine-gabbro TZ30 whereas anorthosite TZ123 is nearly devoid of this oxide (0.46%).

All the gabbros are characterised by high contents in Al_2O_3 negatively correlated with MgO (Fig. 8a): TZ115 and TZ145 are in the range 24–25%, TZ30 and HK188.2 in the range 19–20% and HK533 at 17.7%, the maximum content being reached in the anorthosite (32.3% Al_2O_3). The same negative correlation is observed between MgO and Sr (Fig. 8a). This indicates an important plagioclase cumulus phase within the Tin Zebane mafic rocks which can be roughly evaluated to be in the range 60–70% in the studied gabbros and, as expected nearly only plagioclase in the anorthosite.

The major element composition of the Tin Zebane mafic cumulates can be interpreted as the result of the addition of plagioclase, pyroxenes and olivine. This is shown in Fig. 8 where the concentrations of the minerals measured in Tin Zebane have been reported in addition to whole-rocks (Fig. 8a–d). These diagrams indicate: (1) the anorthosite is always very close to plagioclase. (2) Olivine is a necessary end-member to match the whole-rock compositions for the three gabbros from the layered complex (TZ samples) but only a possibility for the two gabbros from the dyke complex (HK samples). This is particularly clear for MgO (Fig. 8a) and SiO_2 (Fig. 8d). This indicates that the low SiO_2 content in the TZ samples are due to cumulative olivine. This is in agreement with the quite important modal content of olivine in these rocks (12–27%; Table 9). (3) The cpx analysed in the corona has a different composition than the primary cpx, close to opx composition. (4) Amphibole is close to the whole-rocks but always on the opposite side relatively to plagioclase. The addition of plagioclase and amphibole compositions can match the whole-rock composition. (5) The FeO_t concentrations in the two HK samples cannot be matched with the measured mineral compositions, indicating that their higher silica content is due to a more evolved composition of the liquid from which they were produced and that they are not only poorer in cumulate olivine.

In the same way, the abundance of compatible trace elements (Ni and Cr) reflect the cumulated minerals: Cr is ~400 ppm with Ni in the range 170–200 ppm in the gabbros whereas anorthosite contains 131 ppm Cr where as values are below detection limit for Ni (Table 9); Ni and Cr contents are consistent with olivine and pyroxene accumulation.

Chondrite-normalised rare earth element (REE) patterns of Tin Zebane mafic rocks (Fig. 9a) display positive Eu anomalies (Eu/Eu^* from 1.3 to 5.3, 4.05 for the anorthosite) reflecting the abundance of cumulative plagioclase. Laouni troctolitic rocks (Cottin et al., 1998) possess a similar characteristic (Eu/Eu^* from 1.3 to 3.5, with one sample at 0.92). The Tin Zebane mafic rocks have slightly fractionated REE ($La_N/Lu_N = 1.2$–3.9), but LREE and HREE are nearly not fractionated: La_N/Nd_N varies from 0.74 to 1.36 and Dy_N/Lu_N from 1.0 to 1.43. The most silica-rich samples HK188.2 and HK533 have higher abundance of REE ($\Sigma REE = 11$ and 32 ppm) than the other Tin Zebane mafic rocks ($\Sigma REE = 5.2$–10 ppm) and encompass the Laouni range. This indicates that liquids in equilibrium with samples HK188.2 and HK533 were richer in silica and REE.

This similarity of the REE patterns between Laouni troctolites and the most evolved cumulates of Tin Zebane justifies, in a first attempt, to use trace element concentrations measured on Laouni minerals for comparison, as they are not available for Tin Zebane minerals. Plagioclase, clinopyroxene and orthopyroxene spectra from Laouni layered intrusions (Cottin et al., 1998) have then been added for comparison and calculation (Fig. 9b); olivine pattern has been built on the

Table 9
Major and trace element results. G = gabbro; A = anorthosite; OG = olivine-gabbro; LG = leucogabbro

Rock	G	G	A	G	OG	LG	Rock	G	G	A	G	OG	LG
Sample	HK533	HK188.2	TZ123	TZ115	TZ30	TZ145	Sample	HK533	HK188.2	TZ123	TZ115	TZ30	TZ145
SiO_2	47.47	47.08	45.35	44.90	44.24	43.45	qz	0.00	0.00	0.00	0.00	0.00	0.00
TiO_2	1.39	0.93	0.09	0.20	0.13	0.11	or	1.37	6.22	0.00	0.49	0.00	0.00
Al_2O_3	17.65	19.41	32.31	25.27	20.61	24.40	ab	18.68	14.18	10.99	15.52	9.58	10.93
Fe_2O_3	1.05	1.07	0.15	0.46	0.84	0.64	an	37.95	39.31	80.44	61.31	51.06	61.70
FeO	9.43	9.65	1.34	4.11	7.56	5.72	ne	0.00	2.58	2.95	1.00	0.43	0.33
MnO	0.15	0.15	0.00	0.04	0.12	0.07	di wo	10.02	7.42	1.99	1.25	5.08	0.31
MgO	6.92	7.54	0.46	7.38	11.64	9.79	di en	5.30	3.94	0.70	0.84	3.26	0.21
CaO	12.50	11.63	17.06	12.76	12.80	12.44	di fs	4.41	3.25	1.34	0.31	1.48	0.08
Na_2O	2.19	2.26	1.92	2.00	1.22	1.34	hy en	3.03	0.00	0.00	0.00	0.00	0.00
K_2O	0.23	1.06	0.05	0.08	0.05	0.05	hy fs	2.52	0.00	0.00	0.00	0.00	0.00
P_2O_5	0.11	0.03	0.09	0.13	0.13	0.09	ol fo	6.39	10.33	0.32	12.68	18.24	17.33
P.F.	1.09	0.14	1.01	2.52	0.68	1.77	ol fa	5.88	9.41	0.68	5.24	9.11	7.75
Total	100.18	100.95	99.83	99.85	100.02	99.87	mt	1.53	1.54	0.22	0.68	1. 23	0.94
Mg#	0.42	0.44	0.26	0.64	0.61	0.63	ilm	2.67	1.75	0.17	0.39	0.25	0.21
V	302	179	22	35	49	23	ap	0.24	0.06	0.20	0.29	0.29	0.20
Rb	6.4	0.50	2.03	1.99	0.83	0.5		100.00	100.00	100.00	100.00	100.00	100. 00
Y	8.6	3.4	1.9	2.8	2.6	1.25	%pl	58.0	59.7	91.4	77.3	60.6	72.6
Zr	27	6.8	2.84	10.4	3.51	1.5	%ol	12.3	19.7	1.0	17.9	27.3	25.1
Nb	0.6	0.10	0.11	0.27	0.10		%cpx	19.7	14.6	4.0	2.4	9.8	0.6
Ba	244	33	24.1	54.9	11.9	16.1	%opx	5.6	0.0	0.0	0.0	0.0	0.0
Co			3	34	55	47							
Cr			131	379	433	400							
Cu				69	48	13							
Ga			19.2	15.7	12.1	15.5							
Ni			10	193	187	168							
Mo			3.6	1.6	2.3	1.9							
W	0.2	0.1	3.4	1.9	2.9	1.9							
Zn			5.2	26	45	42							
La	4.60	1.50	0.85	1.36	0.42	0.86							
Ce	9.40	3.30	2.06	3.19	1.24	1.99							
Pr	1.40	0.40	0.29	0.44	0.18	0.27							
Nd	6.80	2.20	1.38	2.26	1.10	1.23							
Sm	1.80	0.63	0.31	0.60	0.36	0.30							
Eu	0.83	0.48	0.45	0.43	0.35	0.49							
Gd	2.10	0.78	0.38	0.56	0.39	0.25							
Tb			0.05	0.09	0.06	0.04							
Dy	2.10	0.86	0.31	0.46	0.47	0.23							
Ho	0.41	0.16	0.06	0.10	0.10	0.04							
Er	1.19	0.46	0.20	0.26	0.21	0.12							
Tm			0.03	0.04	0.03	0.02							
Yb	1.09	0.43	0.16	0.25	0.24	0.12							
Lu	0.15	0.06	0.03	0.04	0.04	0.02							
Hf	0.99	0.29	0.09	0.27	0.17	0.05							
Ta	0.1	0.1	0.05	0.05	0.05	0.05							
Pb	5.3	0.27	2.73	1.03	0.74	0.72							
Th	0.33	0.12	0.05	0.05	0.05	0.05							
U	0.05	0.05	0.10	0.05	0.05	0.05							
Sr	442	432	521	480	322	356							
Eu^*/Eu	1.30	2.09	4.05	2.24	2.83	5.29							

Samples HK533 and HK188 from Hadj-Kaddour et al. (1998); Blank = below detection limit.

opx pattern, using their relative K_d (values from the compilation by Rollinson, 1993). The Tin Zebane REE spectra can be reduced nearly to the addition of the cumulus minerals. The slight positive slope of HREE in samples TZ30 and TZ145 can be explained by the presence of orthopyroxene that displays a major enrichment in HREE compared to LREE. As examples (Fig. 9b), the spectrum of the three following samples could correspond to the addition of:

- olivine-gabbro TZ30: 60% pl (variety pl_1) + 37% ol + 11% cpx + 2% opx;
- anorthosite TZ123: 87% pl (78% pl_1 + 9% pl_2) + 3% ol + 7% cpx + 3% opx;

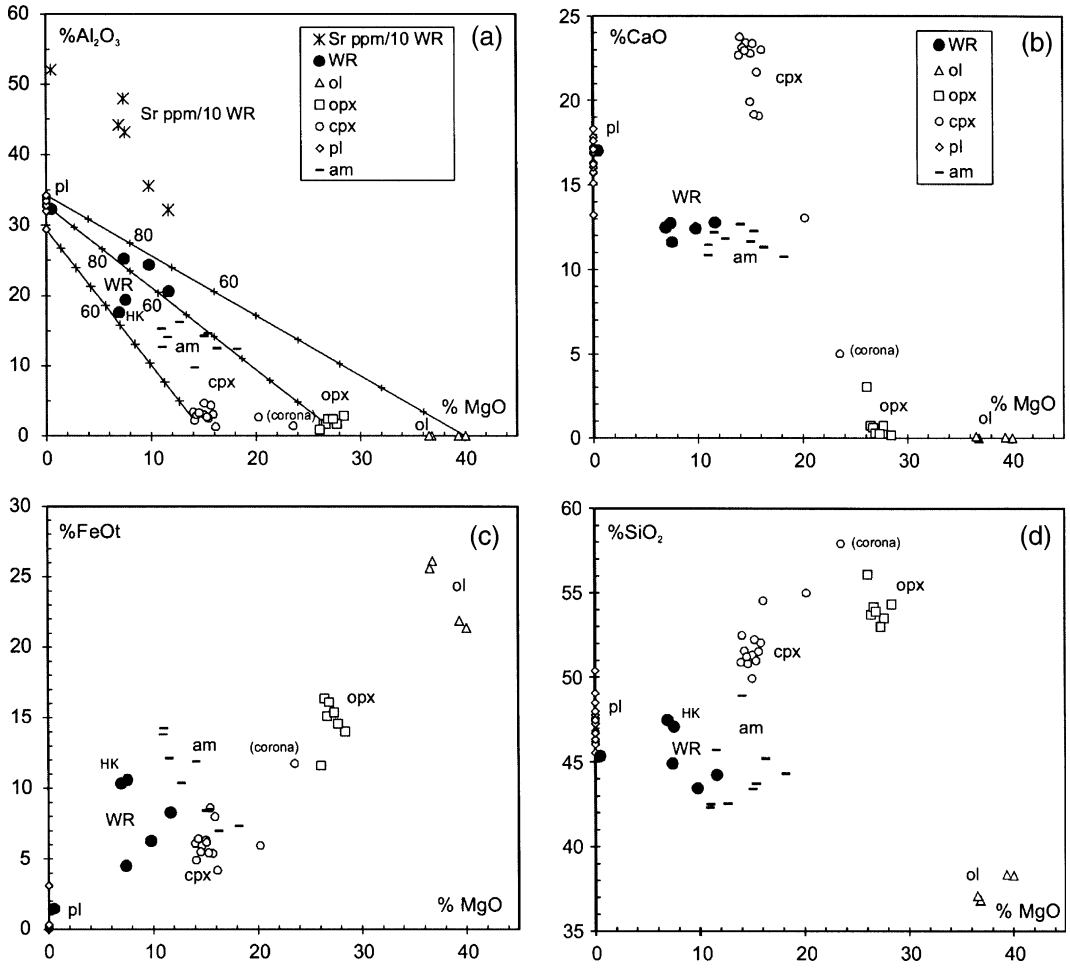

Fig. 8. Whole-rock and minerals from Tin Zebane layered complex: (a) MgO vs. Al_2O_3 and Sr (ppm) divided by 10; (b) MgO vs. CaO; MgO vs. FeO_t; MgO vs. SiO_2.

- high-SiO_2 gabbro HK188.2: 57% pl (70% pl_1 + 17% pl_2) + 20% ol + 20% cpx + 2% opx.

The low proportion of pyroxenes and the limited dilution role played by olivine explain why all cumulates spectra are close to plagioclase spectra and why the spectra of the gabbros are close to that of the anorthosite.

These calculations are highly dependant on the mineral compositions used, here taken from another complex. However, this calculation shows that trace elements can agree with major elements and with the observed petrographic features. This implies that residual liquid is present in very low amounts, if any, and that accessory minerals played a very minor role in the REE fractionation that behaved as incompatible elements at this stage of differentiation. These coherent results indicate that REE remained immobile during the late magmatic development of amphibole and the partial greenschist retrogression of the rocks.

Primitive-mantle-normalised trace-element patterns illustrated in Fig. 9c for gabbros are similar to the Laouni troctolites but with lower abundances for elements from Zr to V and for LREE in some Tin Zebane mafic rocks. The preponderance of plagioclase in Tin Zebane cumulates is reflected by strong Sr and Ba positive anomalies. Here, also, Tin Zebane gabbros and anorthosite have similar spectra, mainly imposed by cumulus plagioclase. All these rocks are plagioclase-rich cumulates, the variation of the other minerals giving rise to the layered intrusion observed. This is in agreement with the composition of plagioclase in anorthosites (e.g., Ashwal, 1993): the Tin Zebane anorthosite–gabbros plagioclases (in the range An_{86-74}) are characteristic of layered mafic intrusions, which are distinct from the massif-type anorthosites that usually contain a more sodic plagioclase (labrador–andesine, An_{35-65}). The positive anomaly in Ti observed in the two SiO_2-rich gabbros suggests that ilmenite appeared at the liquidus. These spidergrams are marked by negative Nb anomalies, but not of Ta. This is probably due to the analytical detection limit (Nb is very low, four samples being at the detection limit of 0.1). Furthermore, Hadj-Kaddour et al. (1998) pointed out the effects of the fergusonite

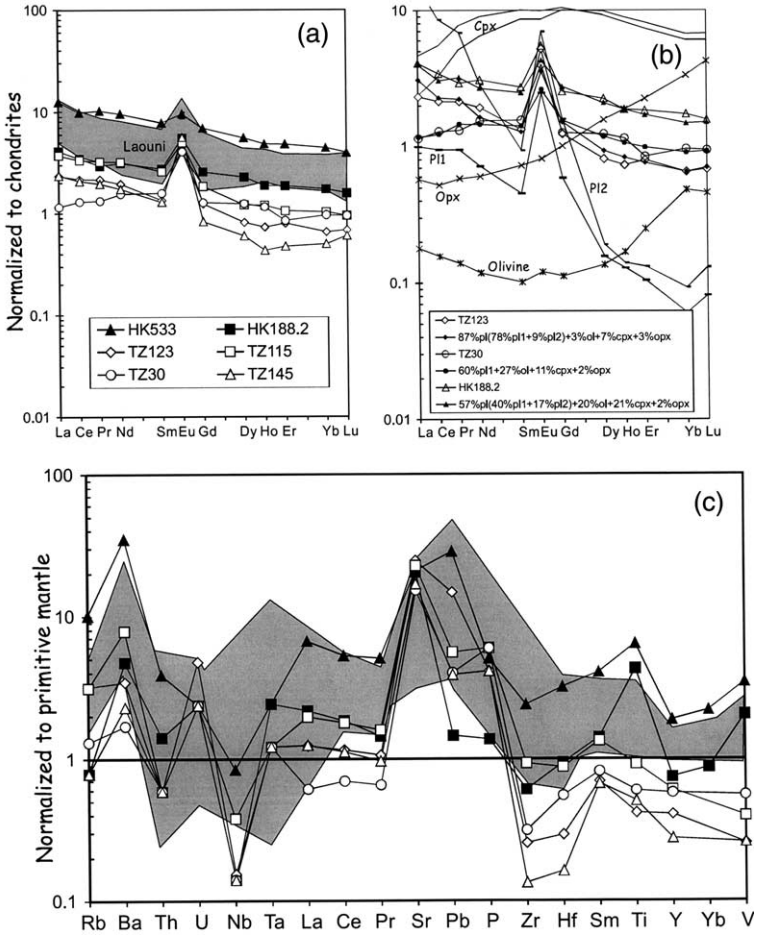

Fig. 9. (a) Chondrite-normalised REE diagram for Tin Zebane mafic rocks compared with the Laouni mafic–ultramafic layered intrusions (Cottin et al., 1998). (b) Modelisation of three Tin Zebane mafic rocks as a mixing of cumulative plagioclase and pyroxenes for REE. Plagioclase and pyroxene compositions from Cottin et al. (1998). (c) Primitive mantle-normalised spidergram for Tin Zebane mafic rocks compared with the Laouni mafic–ultramafic layered intrusions (Cottin et al., 1998).

[(La, Ce, Nd, Y)(Nb,Ta)O_4] crystallisation in the Tin Zebane granitoids, thus a geological cause cannot be entirely excluded.

6. Discussion and conclusion

The Tin Zebane mafic rocks are layered bodies of cumulates composed of varying proportions of plagioclase (mostly $An_{86–74}$), olivine ($Fo_{71–78}$), clinopyroxene (augite-diopside) and orthopyroxene (hypersthene). Fe–Ti oxides (magnetite, ilmenite, exsolved spinel) and rare primary amphibole are also observed within the cumulate texture. After the development of various symplectites, later retrogression is marked by the crystallisation of amphibole and afterwards by greenschist facies mineral growth. Whole-rock geochemistry and Sr–Nd isotopes signature were not significantly affected during these last events. A similar conclusion was reached by Hadj-Kaddour et al. (1998) in the southern part of the complex for the Tin Zebane granitoids often strongly mylonitised and partly retrogressed in greenschist facies conditions. *P–T* conditions were estimated for the late symplectitic–corona texture: ca. 800 °C and 6.2 kbar.

The Sr and Nd isotopic initial ratios point to a depleted mantle source: $Sr_i = 0.70257–0.70278$, $\varepsilon_{Nd} = +5.9$ to +7.8, values identical to the spatially associated alkaline–peralkaline subvolcanic granitoids: $Sr_i = 0.70281 \pm 0.00001$ and $\varepsilon_{Nd} = +6.4 \pm 0.6$ (Hadj-Kaddour et al., 1998). On this basis, the studied mafic rocks and the granitoids are interpreted as cogenetic. The age of 592.2 ± 5.8 Ma (Rb–Sr isochron on 19 granitoids; Hadj-Kaddour et al., 1998) can then be applied to the studied Tin Zebane mafic rocks with a good degree of confidence.

The Tin Zebane mafic rocks correspond to plagioclase-rich cumulates. Their major and trace element geochemistry point to ca. 60% of plagioclase in the studied gabbros, with the extreme case of the anorthosite (ca. 90% plagioclase). Such a cumulative assemblage

dominated by plagioclase was required to account for the Tin Zebane granitoids, particularly for the peralkaline series marked by low Ca, Sr and Al contents (Hadj-Kaddour et al., 1998). The peralkaline granites are indeed poorer in Al_2O_3 rather than richer in $K_2O + Na_2O$ when compared to metaluminous series (Bonin, 1986; Liégeois et al., 1996). The importance of plagioclase fractionation in alkaline series is also attested by large mass of anorthosite in some alkaline ring-complexes e.g. in Aïr–Niger (Black, 1965; Demaiffe et al., 1991).

The presence of granitic liquids and gabbroic cumulates in Tin Zebane complex could be a consequence of an intermediate, monzonitic, parental magma as suggested by Lameyre and Bonin (1978). On the other hand, when dealing only with the mafic cumulates, it is not easy to determine if they belong to an alkaline or a tholeiitic series as both are enriched in iron. Only the differentiated liquids or cumulates will allow the distinction. The similarity (petrography, geochemistry, nature of the mantle source) and differences (variable crustal contamination) existing between the Tin Zebane and the Laouni mafic layered intrusions are close to those existing between the Tin Zebane granitoids and the Taourirt granitoids. This suggests that the Laouni mafic layered intrusions could be genetically linked to the Taourirt granitoids, being the early cumulates of the series, as suggested by Azzouni-Sekkal et al. (2003).

The depleted mantle source and the absence of any crustal contamination within the Tin Zebane complex have been attributed to post-collisional trans-tensional movements along the rigid In Ouzzal terrane (Hadj-Kaddour et al., 1998). This setting can indeed generate a linear lithospheric delamination along the mega-shear zone, allowing the uprise of the asthenosphere that can melt because of an adiabatic pressure release. This asthenosphere is enriched in OIB-type elements. This enrichment could either pre-date the uprise or develop during the ascent of asthenosphere through the lower lithosphere, which is a reservoir likely to be enriched in such elements (Black and Liégeois, 1993). In the Tin Zebane case, the rigidity and coldness of the In Ouzzal rigid terrane would allow the asthenospheric melts to uprise rapidly without long-lived intermediate chambers where crustal contamination is favoured. This rapid upward movement could also explain the presence of cumulates having formed at ca. 20 km depth: they could have been dragged along the shear zone by the liquids that emplaced as dykes. This would explain the recrystallised texture of these rocks and the out of equilibrium composition of the primary mineral phases. The contemporaneous tectonics was not anymore transpressional and generating large horizontal movements but transtensional with limited displacement. This kind of intrusions thus seal the belt boundaries largely in their current positions (Corriveau and Van Breemen, 2000). More to the east, within the LATEA metacraton (Liégeois et al., 2003; Fig. 1), the Laouni layered intrusion magmas would have been generated in a similar manner from the same source but, only a few magma batches could reach the surface without crustal contamination.

Acknowledgements

We thank J.C. Duchesne and L. Corriveau for their careful reviews of the manuscript and their constructive and thoughtful comments which improved the paper. This work is a contribution to projects "Héritage éburnéen et structuration panafricaine du Hoggar: étude géologique et géophysique" supported by the French-Algerian cooperation program 00MDU476 and PNR AU 19943 supported by Andru in Algeria. This is a contribution to IGCP 485 and to NATO project EST/CLG 979766.

References

Abdelsalam, M., Liégeois, J.P., Stern, R.J., 2002. The Saharan metacraton. Journal African Earth Sciences 34, 119–136.

Aït-Djafer et al., 2003. Written communication.

Ashwal, L.D., 1993. Anorthosites. Springer-Verlag, New York. 422 p.

Ashworth, J.R., 1986. The role of magmatic reaction, diffusion and annealing in the evolution of coronitic microstructure in troctolitic gabbro from Risör, Norway: a discussion. Mineralogical Magazine 50, 469–479.

Azzouni-Sekkal, A., Liégeois, J.P., Bechiri-Benmerzoug, F., Belaidi-Zinet, S., Bonin B., 2003. The "Taourirt magmatic province, a marker of the very end of the Pan-African orogeny in the Tuareg Shield: review of the available data and Sr–Nd isotope evidence. Journal of African Earth Sciences, this issue.

Black, R., 1965. Sur la signification pétrogénétique de la découverte d'anorthosites associées aux complexes annulaires sub-volcaniques du Niger. Comptes Rendus de l'Académie des Sciences Paris 260, 5829–5832.

Black, R., Caby, R., Moussine-Pouchkine, A., Bayer, R., Bertrand, J.M.L., Barllier, A.M., Fabre, J., Lesquer, A., 1979. Evidence for late Precambrian plate tectonics in West Africa. Nature 278, 223–227.

Black, R., Latouche, L., Liégeois, J.P., Caby, R., Bertrand, J.M., 1994. Pan-African displaced terranes in the Tuareg shield (central Sahara). Geology 22, 641–644.

Black, R., Liégeois, J.P., 1993. Cratons, mobile belts, alkaline rocks and continental lithospheric mantle: the Pan-African testimony. Journal of Geological Society of London 150, 89–98.

Boissonnas, J., 1974. Les granites à structures concentriques et quelques autres granites tardifs de la chaîne pan-africaine en Ahaggar (Sahara central, Algérie). Thèse d'État, Centre de Recherches sur les Zones Arides, Série Géologie 16, 662 p.

Bonin, B., 1986. Ring complex granites and anorogenic magmatism. In: Studies in Geology. North Oxford Academic, Oxford, and Elsevier, Amsterdam. 188 p.

Boullier, A.M., Liégeois, J.P., Black, R., Fabre, J., Sauvage, M., Bertrand, J.M., 1986. Late Pan-African tectonics marking the transition from subduction-related calc-alkaline magmatism to within-plate alkaline granitoids (Adrar des Iforas, Mali). Tectonophysics 132, 233–246.

Caby, R., 1970. La chaine pharusienne dans le NW de l'Ahaggar (Sahara central; Algérie): sa place dans l'orogenèse du Précambrien supérieur en Afrique. Thesis, University of Monpellier, France, 335 p.

Caby, R., Andreopoulos-Renaud, U., 1983. Age à 1800 Ma du magmatisme sub-alcalin associé aux métasédiments monocycliques dans la chaine Pan-Africaine du Sahara central. Journal of African Earth Sciences 1, 193–197.

Caby, R., Andreopoulos-Renaud, U., Pin, C., 1989. Late Proterozoic arc-continent and continent-continent collision in the Pan-African Trans-Saharian belt of Mali. Canadian Journal of Earth Sciences 26, 1136–1146.

Caby, R., Monié, P., 2003. Neoproterozoic subduction and differential exhumation of western Hoggar (southwest Algeria): new structural, petrological and geochronological evidence. Journal of African Earth Sciences, this issue.

Corriveau, L., Van Breemen, O., 2000. Docking of the central metasedimentary belt to Laurentia in geon 12: evidence from the 1.17–1.16 Ga Chevreuil intrusive suite and host gneisses, Quebec. Canadian Journal of Earth Sciences 37, 253–269.

Cottin, J.Y., Lorand, J.P., Agrinier, P., Bodinier, J.L., Liégeois, J.P., 1998. Isotopic (O, Sr, Nd) and trace element geochemistry of the Laouni layered intrusions (Pan-African belt, Hoggar, Algeria): evidence for post-collisional continental tholeiitic magmas variably contaminated by continental crust. Lithos 45, 197–222.

Demaiffe, D., Moreau, C., Brown, B., Weis, D., 1991. Geochemical and isotopic (Sr, Nd and Pb) evidence on the origin of anorthosite-bearing anorogenic complexes of the Aïr province, Niger. Earth Planetary Science Letters 105, 28–46.

Dostal, J., Caby, R., Dupuy, C., 1979. Metamorphosed alkaline intrusions and dyke complexes within the Pan-African belt of western Hoggar (Algeria): geology and geochemistry. Precambrian Research 10, 1–20.

Dostal, J., Caby, R., Dupuy, C., Mével, C., Owen, J.V., 1996. Inception and demise of Pre-Pan-African ocean basin: evidence from the Ougda complex, Western Hoggar (Algeria). Geologische Rundschau 85, 619–631.

Hadj-Kaddour, Z., Liégeois, J.P., Demaiffe, D., Caby, R., 1998. The alkaline–peralkaline granitic post-collisional Tin Zebane dyke swarm (Pan-African Tuareg shield, Algeria): prevalent mantle signature and late agpaitic differentiation. Lithos 45, 223–243.

Holland, T.J.B., Blundy, J.D., 1994. Non-ideal interactions in calcic amphiboles and their bearing on amphibole plagioclase thermometry. Contributions to Mineralogy and Petrology 116, 433–447.

Holland, T.J.B., Powell, R., 1998. An internally consistent thermodynamic data set for phases of petrological interest. Journal of Metamorphic Geology 16, 309–343.

Jahn, B.M., Caby, R., Monié, P., 2001. The oldest UHP eclogites of the world: age of UHP metamorphism, nature of protoliths and tectonic implications. Chemical Geology 178, 143–158.

Joesten, R., 1986. The role of magmatic reaction, diffusion and annealing in the evolution of coronitic microstructure in troctolitic gabbro from Risör, Norway. Mineralogical Magazine 50, 441–467.

Kienast, J.R, Ouzegane, K., 1987. Polymetamorphic Al–Mg rich parageneses in Archean rocks from Hoggar, Algeria. Geological Journal 22, 57–79.

Kienast, J.R., Fourcade, S., Guiraud, M., Hensen, B.J., Ouzegane, K. (Eds.), 1996. Special Issue on the In Ouzzal granulite unit, Hoggar, Algeria Journal of Metamorphic Geology 14, 659–808.

Kretz, R., 1983. Symbols for rock-forming minerals. American Mineralogist 68, 277–279.

Lameyre, J., Bonin, B., 1978. Réflexions sur la position et l'origine des complexes magmatiques anorogéniques. Bulletin de la Société géologique de France 20, 45–59.

Leake, B.E., Woolley, A.R., Birch, W.D., Gilbert, M.C., Grice, J.D., Hawthorne, F.C., Kato, A., Kisch, H.J., Krivovichev, V.G., Linthout, K., Laird, J., Mandarino, J., Maresch, W.V., Nickel, E.H., Rock, N.M.S., Schumacher, J.C., Smith, D.C.N., Ungaretti, L., Whittaker, E.J.W., Youzhi, G., 1997. Nomenclature of amphiboles. Canadian Mineralogist 9, 623–651.

Liégeois, J.P., Bertrand, J.M., Black, R., 1987. The subduction and collision-related Pan-African composite batholith of the Adrar des Iforas (Mali): a review. Geological Journal 22, 185–211.

Liégeois, J.P., Black, R., Navez, J., Latouche, L., 1994. Early and late Pan-African orogenies in the Aïr assembly of terranes (Tuareg shield Niger). Precambrian Research 67, 59–88.

Liégeois, J.P., Diombana, D., Black, R., 1996. The Tessalit ring complex (Adrar des Iforas, Malian Tuareg shield): a Pan-African, post-collisional, syn-shear, alkaline granite intrusion. In: Demaiffe, D. (Ed.), Petrology and Geochemistry of Magmatic Suite of Rocks in the Continental and Oceanic Crusts. ULB-MRAC, Bruxelles, pp. 227–244.

Liégeois, J.P., Latouche, L., Boughrara, M., Navez, J., Guiraud, M., 2003. The LATEA metacraton (Central Hoggar, Tuareg shield, Algeria): behaviour of an old passive margin during the Pan-African orogeny. Journal of African Earth Sciences, this issue.

Liégeois, J.P., Navez, J., Hertogen, J., Black, R., 1998. Contrasting origin of post-collisional high-K calc-alkaline and shoshonitic versus alkaline and peralkaline granitoids. The use of sliding normalization. Lithos 45, 1–28.

Ludwig, K.R., 1999. Using Isoplot/Ex Version 2.01, A Geochronological Toolkit for Microsoft Excel. Berkeley Geochronology Center Special Publication 1a, 47 p.

Ouzegane, K., Kienast, J.R., Bendaoud, A., Drareni, A., 2003. A review of Archaean and Paleoproterozoic evolution of the In Ouzzal granulitic terrane (Western Hoggar, Algeria). Journal of African Earth Sciences, this issue.

Pin, C., Briot, D., Bassin, C., Poitrasson, F., 1994. Concomitant separation of strontium and samarium–neodymium for isotopic analysis in silicate samples, based on a specific extraction chromatography. Analytica Chimica Acta 298, 209–217.

Rollinson, H., 1993. Using Geochemical Data: Evaluation, Presentation, Interpretation. Longman Scientific and Technical, Harlow, Great Britain. 352 p.

Zindler, A., Hart, S.R., 1986. Chemical geodynamics. Annual Review of Earth and Planetary Sciences 14, 493–571.